Mass transfer characteristics through alumina membranes with different pores sizes and porosity.

OGUNLUDE, P., ABUNOMAH, O., HASHIM, I., AISUENI, F., OGOUN, E., ANTWI, S., RAMALAN, M., WILLIAMWEST, T., SUKKI, F.M. and GOBINA, E.

2022

International Journal on Engineering, Science and Technology
Volume 4, Issue 1, 2022 ISSN: 2642-4088

Mass Transfer Characteristics through Alumina Membranes with Different Pores Sizes and Porosity

Priscilla Ogunlude
Robert Gordon University, United Kingdom

Ofasa Abunomah
Robert Gordon University, United Kingdom

Idris Hashim
Robert Gordon University, United Kingdom

Florence Aisueni
Robert Gordon University, United Kingdom

Evans Ogoun
Robert Gordon University, United Kingdom

Samuel Antwi
Robert Gordon University, United Kingdom

Muktar Ramalan
Robert Gordon University, United Kingdom

Tamunotonye Williamwest
Robert Gordon University, United Kingdom

Firdaus Muhammad Sukki
Edinburgh Napier University, United Kingdom

Edward Gobina
Robert Gordon University, United Kingdom, e.gobina@rgu.ac.uk

Abstract: Different membranes covering the macroporous to nano-pororous range and having different porosities have been used to study the mass transfer of methane and carbon dioxide single gases. The effect of flow parameters on the transport mechanisms through porous membranes were reviewed in detail. The characteristics of gas transport through the macroporous, microporous, and nano-porous membranes were investigated with several gas diffusion models in the range of 20–100 ◦C and at pressure differences ranging from 0.2 to 3 bar. The experimental gas permeation data of the membranes were analyzed using the Darcy flow model. The results clearly showed good agreement between the model analysis and the experimental data. The experimental data showed that the permeation followed a parallel flow model in which the behavior of gases was governed by viscous and Knudsen diffusion, although to varied degrees. Permeation of the gases through each membrane varies considering the viscosity of the gases at the same temperature. Furthermore, the membranes followed the configurational diffusion model in which the permeance increased with increasing pressure and decreasing temperature. For the gas flow measurements through macroporous and nano-porous membranes with diameters ranging from 6000nm to 15nm, the results indicate that the experimental flux agrees well with the calculated (model) flux through which gas flows from the bulk stream in the shell side to the membrane outer surface where viscous flow and Knudsen diffusion coexist. The study shows that experimental flux is larger than Knudsen diffusion, and the contribution of Knudsen diffusion to the experimental flux increases with the decrease in the diameter. On the other hand, the effects of gas slippage are considerable as gas velocity near the wall is higher than zero. The slip length effects are inversely proportional to pore size and with driving pressure.

Keywords: Macroporous, microporous, nano-porous, mass transfer, gas transport, mechanisms, membrane

Introduction

The transport of different constituents in a membrane is depended on the mechanism by which the constituents are transported. As an example, in a porous ceramic membrane the various constituents are transported because of the pressure difference established between the feed side and permeate side. In polymeric membrane systems in general the solution diffusion transport operates. The permeability of these membranes is controlled by the diffusivities and concentrations of the various constituents in the membrane matrix and the rates of transport are generally comparatively slow. In porous membrane systems however, mass is transferred because of the driving force of the hydrostatically established difference in pressure and can be viscous, Knudsen, capillary condensation, nano-porous mechanism (1 – 4) as shown in Figure 1.

The separation and application of porous ceramic membrane depends on its pore size, as shown in Figure 1. In this study we will concentrate on inorganic membranes. Inorganic ceramic membranes, currently are currently being used for ultrafiltration and microfiltration, are made from aluminium (α-Al_2O_3, γ-Al_2O_3), silica (SiO_2) or titanium (TiO_2) oxides. At elevated temperatures ceramic membranes have the advantages over polymer ones, showing mechanical stability, chemical inertness, and corrosion resistance. This stability allows ceramic microfiltration-ultrafiltration membrane to be applicable for gas separation under high pressure and high temperature conditions. According to Baker (8), pore diameters in ceramic membranes for microfiltration and ultrafiltration range from 0.01 to 10 μm. These membranes are generally used as the base support for depositing gas separating layers and are made by a dip coating-sintering procedure. In addition, sol-gel methods are used to produce membranes with pores from 10 to 100 Å.

Ceramic membranes are classified into two types based on its morphology: dense and porous (especially microporous) ceramic membranes. Dense membranes consist of crystalline ceramic materials such as perovskites or fluorites and include metals such as palladium or palladium alloys. Membranes made of such materials are characterized by the ability to allow permeation of only hydrogen or oxygen through itself, providing an extremely high selectivity towards these two gases. Consequently, they are mostly not applicable in selective transport of all other gases. For a porous ceramic membrane, their gas transport is mostly controlled by pore size, thickness, and surface porosity of the membrane, whereas in dense ceramic membranes permeation and separation are governed by more complex principles [5].

Permeability Coefficient

The permeability coefficient, denoted as P (or simply referred to as the permeability) is defined as the permeate flux of material through the membrane per unit driving force per unit membrane area per unit membrane thickness. P must be determined experimentally. The Barrer is the commonly used unit for gas permeability, and it is defined as:

$$1 \text{ Barrer} = 10^{-10} \text{ (cm}^3\text{@STP/cm}^2\text{.s-Hg)} \quad (1)$$

The term cm^3@STP/cm^2.s denotes the volumetric flux across the membrane of the diffusing constituent at standard conditions of 0^oC and 1 atm, the cm refers to the thickness of the membrane separation layer, and cm-Hg denotes the partial pressure difference across the membrane for the diffusing constituent. Other often used units are: kmol.m.m^{-2}.s^{-1}.kPa^{-1}, or m^3.m.m^{-2}.s^{-1}.kPa^{-1}, or kg. m.m^{-2}.s^{-1}.kPa^{-1} and it is generally recognized that the driving force in these variants is the pressure difference across the membrane.

Permeance

The permeance F_T is defined as the ratio of the permeability coefficient (P) to the membrane thickness (δ). The permeance for a given constituent diffusing through a membrane with a defined thickness is analogous to a mass transfer coefficient

Membrane Selectivity ($\alpha_{A/B}$)

In the separation involving gases, the membrane selectivity is used as a comparator of the separating efficiency of a membrane for 2 or more species. The membrane selectivity, αA/B is therefore also known as the perm-selectivity for one component (A) over another component (B) and is given by the ratio of their respective permeabilities:

$\alpha_{A/B} = P_A/P_B$ (2)

Selectivity obtained from ratio of permeabilities of the pure gases as shown in equation 2 is known as the ideal membrane selectivity or the ideal perm-selectivity. This is described as an intrinsic property of the membrane material. If a membrane had pores of the same diameter, then the molecules whose diameters were smaller than the diameter of the pore would pass through the membrane, and those molecules having diameters larger than the pore diameter would be totally excluded. Such a membrane would typically show an infinite selectivity. Therefore, the selectivity will range from 1 (for the macroporous systems) to infinity (for the completely dense systems having no pinholes and cracks) when PB = 0.0. Therefore, dense membrane systems possess infinite selectivity but low permeance, while porous systems have high permeance with low to moderate selectivity (Figure 1).

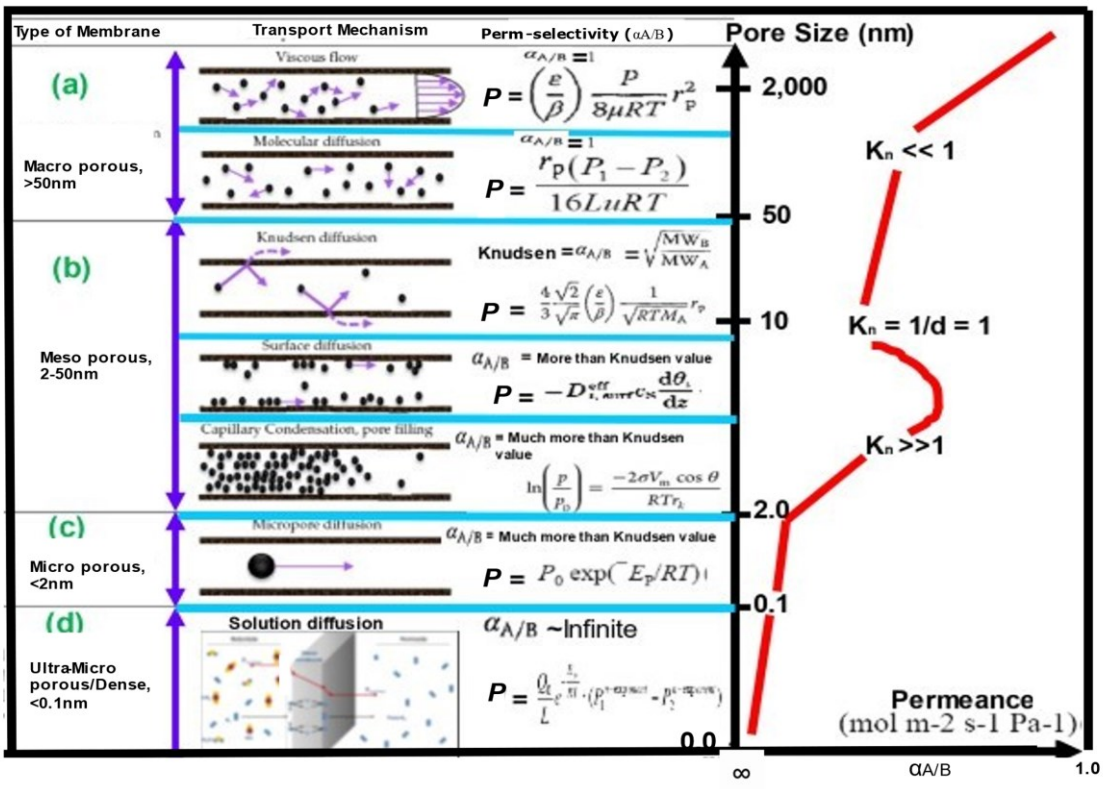

Figure 1. Gas Transport Mechanisms in Porous Media

The selectivity of real-life membranes is usually less than infinite due to many factors. First, seldom will all pores in a membrane be the same size (although systems such as acid etched Vycor glass can approach such uniformity (6) and research is being carried out towards achieving this goal using carbon membranes (7). Thus, without such uniformity the smaller pores might exclude one component in the mixture while larger pores allow it to pass through. In such a case, the selectivity would depend on the relative populations of various pore sizes or distribution. Second, some molecules may be able to deform to some extent and could enter pores that are slightly smaller than their original diameter. Third, molecules of one constituent may adsorb on the walls of the pores and therefore reduce the effective diameters of these pores. In such a case the pore's effective diameter might vary with the feed/retentate and permeate compositions, depending on the concentration of the stronger adsorbing constituent in each of the streams.

It is also important to note that in practical membrane gas separation operations gas mixtures are used rather than pure gases. If the gases in a mixture do not have strong interactions with the membrane material, then the pure gas intrinsic selectivity and the gas mixture selectivity will be identical. This is usually found for mixtures of O_2 and N_2. Gas mixtures are also usually non-ideal, especially under elevated pressure, and thus the actual selectivity may deviate significantly from the ideal value. In many cases, such as the mixture of CO_2 and CH_4, the CO_2 is significantly absorbed by the membrane to the extent that the permeability of CH_4 is affected. The selectivity for such a gas mixture will therefore deviate from the calculated selectivity from pure gas value.

Nonetheless, most studies report on ideal selectivity because the pure gas permeabilities are more readily available.

Membrane technology is widely practiced for large-scale industrial applications. For example, membrane plants with ~100,000 m^{-2} membranes have been constructed to treat ~1 billion standard ft^3/day natural gas by removing CO_2 (8,9). The cost of membrane skids is usually a significant portion of the overall cost of membrane plants and scales almost linearly with the membrane area (8,10). The growth in membrane industrial applications has partially benefited from continuous improvements in membrane permeance to reduce the membrane areas required and thus, the associated costs (9,11). Industrial membranes are often graded having a composite structure which comprises a thin selective layer on top of a microporous support on top of a microporous support. The thin film is a smooth surface having good mechanical strength (10). The porous supports are often made of low-cost and high-permeability porous structures such as TiO_2, ZrO_2 or Al_2O_3 for inorganics and poly(ether sulfone) (PES) and polysulfone (PSf) for organics. The support surface often has a porosity of 1−10% and pore radii of 10−100 nm for polymeric membranes and 12,000 - 6,000nm pore size and 4-30% porosity for inorganic membranes. These supports generally conduct the permeated flow with negligible resistance (8,9). In inorganic membranes, at ultra-micropores the permeance is low, but increase as pore sizes increase and depending on the Knudsen number, Kn. as shown in Figure 1.

Experimental

Permeability was measured by the classical steady-state flow method in which a differential pore pressure, ΔP or tans-membrane pressure drop is maintained and the flow rate flowing out from the downstream or permeate side of the samples is monitored using an electronic flowmeter. The ΔP was controlled by the gas regulator for gas permeability measurement and the downstream pressure was released to atmospheric pressure, assumed constant of 0.1 MPa. The two most important performance indicators for a gas separation membrane are the permeance and ideal selectivity (or perm-selectivity). A simple, quick, and very effective way to obtain gas permeance is to apply a gas overpressure to membrane feed side and measure gas flow rate through the membrane on the permeate side at atmospheric pressure (single gas permeance measurement). Then, gas permeance can be estimated using the following expression:

$$Pi = Fi\delta/(A\Delta P) \quad (3)$$

Where:
Pi = Permeability of component i ($m^3.m.m^{-2}.s^{-1}.kPa^{-1}$)
Fi = Permeate flowrate of component i ($m^3.s^{-1}$)
A = Membrane area (m^2)
ΔP = Trans-membrane pressure drop (kPa)
δ = membrane separation layer thickness (m)

Flux values calculated from experimental measurements of flowrate as a function of different pressure drop ΔP for each gas at different temperatures for the different membranes are presented in Table 1-6.

Table 1. Experimental Results for 15nm Pore Size Membrane at 20°C

Inlet Pressure (Pa)	CH4 Outlet Flowrate at 20 degrees (LPM)	CO2 Outlet Flowrate at 20 degrees (LPM)	CH4 Outlet Flowrate at 20 degrees (m3/s)	CO2 Outlet Flowrate at 20 degrees (m3/s)	CH4 Flux (m3/m2/s)	CO2 Flux (m3/m2/s)
0.00000	0.00000	0.00000	0.00000	0.00000	0.00000	0.00000
20000	1.37	0.94	2.2833E-05	1.5667E-05	0.00254439	0.00174578
60000	3.38	2.21	5.6333E-05	3.6833E-05	0.00627739	0.00410445
100000	4.97	3.2	8.2833E-05	5.3333E-05	0.00923037	0.00594309
140000	6.46	4.2	0.00010767	0.00007	0.01199762	0.00780031
180000	7.89	4.68	0.0001315	0.000078	0.01465344	0.00869178
220000	9.47	6.13	0.00015783	0.00010217	0.01758785	0.01138474
260000	10.89	7.05	0.0001815	0.0001175	0.02022509	0.01309338
300000	12.37	8.01	0.00020617	0.0001335	0.02297378	0.01487631

Table 2. Experimental Results for 200nm Pore Size Membrane at 20°C

Inlet Pressure (Pa)	CH4 Outlet Flowrate at 20 degrees (LPM)	CO2 Outlet Flowrate at 20 degrees (LPM)	CH4 Outlet Flowrate at 20 degrees (m3/s)	CO2 Outlet Flowrate at 20 degrees (m3/s)	CH4 Flux (m3/m2/s)	CO2 Flux (m3/m2/s)
0.00000	0.00000	0.00000	0.00000	0.00000	0.00000	0.00000
20000	1.57	1.17	2.6167E-05	0.0000195	0.00250399	0.00186603
60000	3.64	2.4	6.0667E-05	0.00004	0.00580542	0.00382775
100000	5.27	3.42	8.7833E-05	0.000057	0.0084051	0.00545455
140000	6.87	4.45	0.0001145	7.4167E-05	0.01095694	0.00709729
180000	8.42	5.5	0.00014033	9.1667E-05	0.01342903	0.00877193
220000	10.05	6.51	0.0001675	0.0001085	0.01602871	0.01038278
260000	11.58	7.47	0.000193	0.0001245	0.0184689	0.01191388
300000	12.8	8.52	0.00021333	0.000142	0.02041467	0.01358852

Table 3. Experimental Results for 6000nm Pore Size Membrane at 20°C

Inlet Pressure (Pa)	CH4 Outlet Flowrate at 20 degrees (LPM)	CO2 Outlet Flowrate at 20 degrees (LPM)	CH4 Outlet Flowrate at 20 degrees (m3/s)	CO2 Outlet Flowrate at 20 degrees (m3/s)	CH4 Flux (m3/m2/s)	CO2 Flux (m3/m2/s)
0.00000	0.00000	0.00000	0.00000	0.00000	0.00000	0.00000
20000	1.61	1.17	2.6833E-05	0.0000195	0.00118784	0.00086321
60000	3.54	2.24	0.000059	3.7333E-05	0.00261178	0.00165265
100000	5.07	3.31	0.0000845	5.5167E-05	0.00374059	0.00244208
140000	6.53	4.15	0.00010883	6.9167E-05	0.00481777	0.00306183
180000	7.97	5.17	0.00013283	8.6167E-05	0.00588018	0.00381437
220000	9.45	6.13	0.0001575	0.00010217	0.00697211	0.00452265
260000	10.85	7.03	0.00018083	0.00011717	0.00800502	0.00518666
300000	12.32	7.95	0.00020533	0.0001325	0.00908957	0.00586543

Table 4. Experimental Results for 15nm Pore Size Membrane at 100°C

Inlet Pressure (Pa)	CH4 Outlet Flowrate at 100 degrees (LPM)	CO2 Outlet Flowrate at 100 degrees (LPM)	CH4 Outlet Flowrate at 100 degrees (m3/s)	CO2 Outlet Flowrate at 100 degrees (m3/s)	CH4 Flux (m3/m2/s)	CO2 Flux (m3/m2/s)
0.00000	0.00000	0.00000	0.00000	0.00000	0.00000	0.00000
20000	1.34	0.9	2.2333E-05	0.000015	0.00248867	0.0016715
60000	3.31	2.13	5.5167E-05	0.0000355	0.00614739	0.00395587
100000	4.73	3.13	7.8833E-05	5.2167E-05	0.00878464	0.00581309
140000	6.27	4.09	0.0001045	6.8167E-05	0.01164475	0.00759602
180000	7.75	5.05	0.00012917	8.4167E-05	0.01439343	0.00937895
220000	9.29	6.02	0.00015483	0.00010033	0.01725355	0.01118045
260000	10.86	6.97	0.000181	0.00011617	0.02016938	0.0129448
300000	12.44	7.96	0.00020733	0.00013267	0.02310378	0.01478345

Table 5. Experimental Results for 200nm Pore Size Membrane at 100°C

Inlet Pressure (Pa)	CH4 Outlet flowrate at 20 degrees (LPM)	CO2 Outlet flowrate at 20 degrees (LPM)	CH4 Outlet flowrate at 100 degrees (m3/s)	CO2 Outlet flowrate at 100 degrees (m3/s)	CH4 Flux (m3/m2/s)	CO2 Flux (m3/m2/s)
0.00000	0.00000	0.00000	0.00000	0.00000	0.00000	0.00000
20000	1.61	1.09	2.6833E-05	1.8167E-05	0.00256778	0.00173844
60000	3.64	2.39	6.0667E-05	3.9833E-05	0.00580542	0.0038118
100000	5.22	3.37	0.000087	5.6167E-05	0.00832536	0.0053748
140000	6.85	4.39	0.00011417	7.3167E-05	0.01092504	0.00700159
180000	8.45	5.45	0.00014083	9.0833E-05	0.01347687	0.00869219
220000	10.03	6.53	0.00016717	0.00010883	0.01599681	0.01041467
260000	11.63	7.57	0.00019383	0.00012617	0.01854864	0.01207337
300000	12.8	8.59	0.00021333	0.00014317	0.02041467	0.01370016

Table 6. Experimental Results for 6000nm Pore Size Membrane at 100°C

Inlet Pressure (Pa)	CH4 Outlet flowrate at 100 degrees (LPM)	CO2 Outlet flowrate at 100 degrees (LPM)	CH4 Outlet flowrate at 100 degrees (m3/s)	CO2 Outlet flowrate at 100 degrees (m3/s)	CH4 Flux (m3/m2/s)	CO2 Flux (m3/m2/s)
0.00000	0.00000	0.00000	0.00000	0.00000	0.00000	0.00000
20000	1.68	1.05	0.000028	0.0000175	0.00123949	0.00077468
60000	3.56	2.31	5.9333E-05	0.0000385	0.00262653	0.00170429
100000	5.02	3.18	8.3667E-05	0.000053	0.0037037	0.00234617
140000	6.44	4.23	0.00010733	0.0000705	0.00475136	0.00312085
180000	7.95	5.14	0.0001325	8.5667E-05	0.00586543	0.00379224
220000	9.45	6.04	0.0001575	0.00010067	0.00697211	0.00445625
260000	10.95	6.96	0.0001825	0.000116	0.0080788	0.00513502
300000	12.36	7.95	0.000206	0.0001325	0.00911908	0.00586543

Results and Discussion

Membrane Geometric Structure

In our membranes the membrane layers are fixed on the support, starting with very coarse layers – so called gutter, then followed by the intermediate layers and membrane layers with decreasing pore sizes are added until the designated pore sizes are reached as shown in Figure 2. It shows a scanning electron micrograph and an illustration of the layered arrangement in a typical structure. The layers are usually made from different materials such as aluminium oxide (Al_2O_3), titanium oxide (TiO_2), zirconium oxide (ZrO_2), silicon dioxide (SiO_2), silicon carbide (SiC), Zeolite or a hybrid mixture of two or more materials for the fabrication of different layers of the composite ceramic membranes and are carefully selected so that they are thermally compatible with the support to prevent delamination or crack formation at elevated temperatures. Design of the membrane itself can employ the use of sol gel technique which modifies the pore size of the membrane with high level superficial area through dip-coating process. The crucial part of dip-coating process is the preparation of membrane-forming suspension which mainly consists of ceramic powders and other additives such as binders, dispersants, and plasticizers. With higher environmental protection criteria implemented, aqueous membrane-forming suspension is becoming increasingly common for being eco-friendly and of low-cost compared to organic solvents. Adversely certain disadvantages are commonly confronted in a water-based system, leading to the poor performances of the final products. These negative consequences include a long drying time and high crack sensitivity, due to the huge surface tension of water. Some advantages of sol gel technique include a nanometre scale pore size distribution, homogenous pore size distribution and fabrication of a top layer capable of a comprehensive pore size control. One major complexity encountered during membrane fabrication is on how to tackle the relationship between getting high flux and high selectivity materials. This can be attributed to the inverse proportionality of flow rate to membrane layer thickness. For example, to achieve a membrane with the pore size of 200nm, the support will have layer 1 to achieve a macroporous membrane, while a membrane

with pore size of 200nn also macroporous will have the support plus layer 1 and layer 2. To get a membrane with mesoporous size of 15 nm, we will have the support plus layers 1 + 2 + 3. Subsequent pore size reductions to get to the microporous size will add the top layer on this structure to get down to < 2nm.

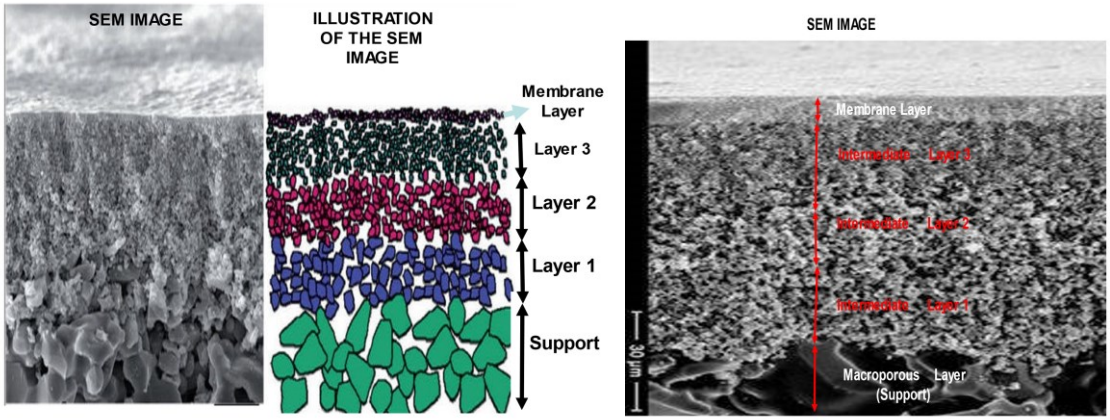

Figure 2. Scanning Electron Microscopy and Illustration of the Layered Ceramic Membrane

Effect of Porosity and Tortuosity on Permeance

Table 7 shows the properties of the membranes used in the study. As shown in Figure 3-6, increasing porosity increases the membrane permeance efficiency. However, there seems to be an optimum porosity of about 15% beyond which efficiency tends to fall. At a typical support porosity of 0.05 and a scaled selective layer thickness of 2, the permeance efficiency is as low as 0.17, indicating a significant flux restriction imposed by the porous support. Porosity and Permeability are the terms related to rocks and soils as both are the measurement regarding them. Porosity is the measurement of void spaces between rocks, whereas permeability is the measurement which tells how easily fluid can flow in between rocks. Porosity is a complex measurement which is taken out after taking various samples from the scene. Two of the famous methods used for measuring porosity are Archimedes method and Boyle's Law. On the other hand, Darcy's Law is the most prominent method used to measure the permeability. Membrane porosity was calculated using particulate density while tortuosity was calculated from previous studies on image analysis and numerical simulations with values stated in Table 7 (12).

Table 7. Morphological Properties of the Membranes used in the Experiment

Membrane pore size, nm	porosity	tortuosity	Ratio of porosity to tortuosity
15	0.13	3.47	0.0375
200	0.20	3.23	0.0619
6000	0.04	3.77	0.0106

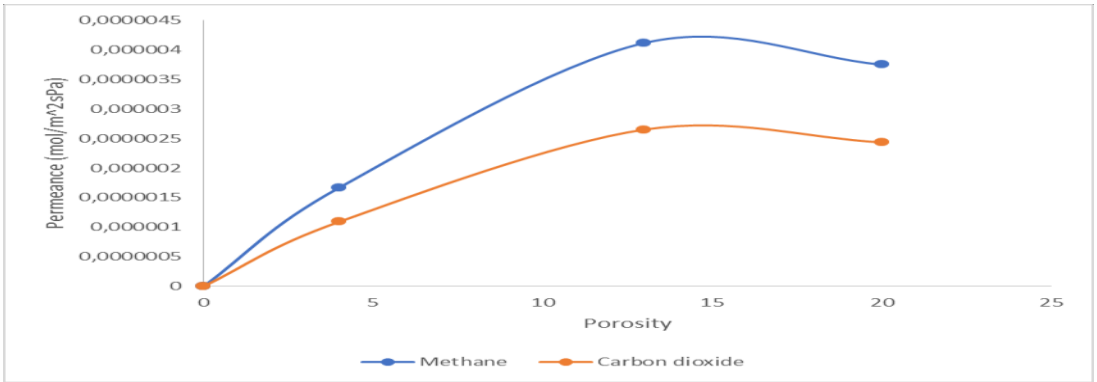

Figure 3. Effect of Porosity on Permeance at 1bar and 20^{o}C

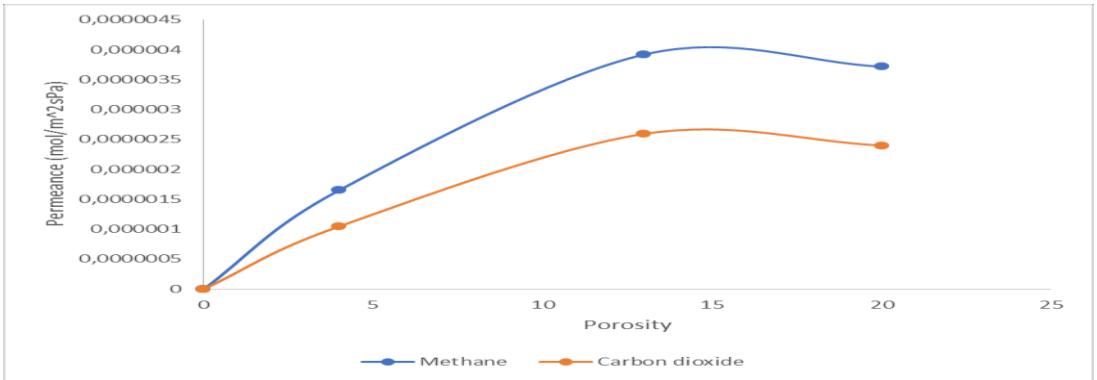

Figure 4. Effect of Porosity on Permeance at 1bar and 100°C

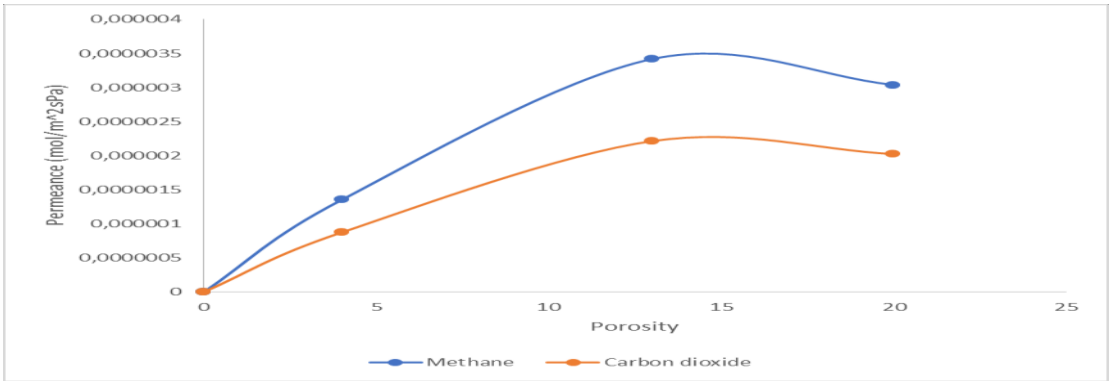

Figure 5. Effect of Porosity on Permeance at 3bar and 20°C

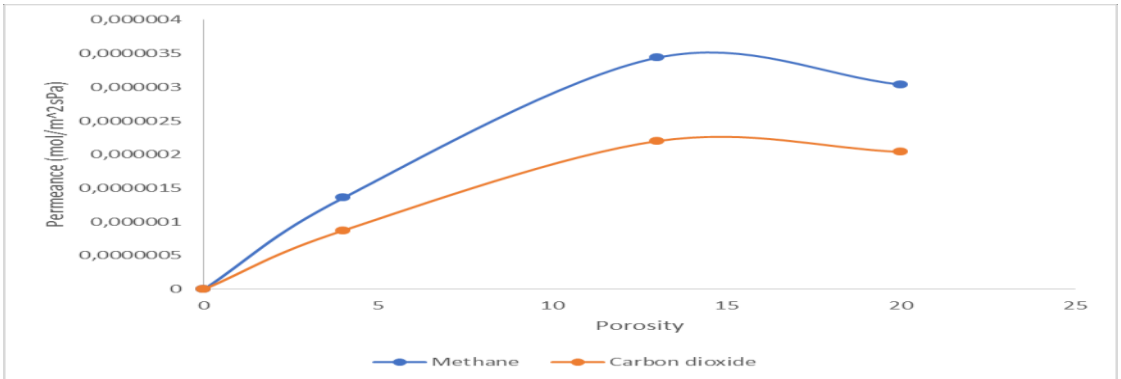

Figure 6. Effect of Porosity on Permeance at 3bar and 100°C

Effect of Pressure and Temperature on Permeance

Gas permeance strongly depends on the operating temperature and can also be affected by the trans-membrane pressure. Therefore, measurements under different process conditions have been carried out for a detailed membrane evaluation. At this juncture, it must be emphasised that gas permeance, typically expressed in mol/m^2 s Pa, is characteristic specific to the membrane tested and is dependent on the thickness of the diffusion barrier, in contrast with permeability, typically expressed in mol/m s Pa, which is characteristic of the material of the membrane and therefore independent on the thickness of the diffusion layer. By measuring gas permeance of two different single gases (CO2 and CH4), the ideal selectivity of a gas pair can be evaluated as detailed in equation 2 earlier. The gas permeance of a membrane is related to the membrane area needed for a certain productivity, whereas the ideal selectivity of a membrane is related to the purity of the final product. Figure 7 - 9 shows that we need more pressure drop for same o flow rate above a pressure drop of 100,000 Pa. Inertia is the resistance to any change in its state of motion including changes to its speed and direction or the state of rest. It is the tendency of objects to keep moving in a straight line at constant velocity. Turbulent flow is due to high flow rate due to increase in pressure difference, gas molecule continuously changes its direction and pore cross

section area due to pressure difference close to bore. Under these conditions, conventional streamlines flow becomes very difficult to obtain and more pressure drop require flowing which make it turbulent.

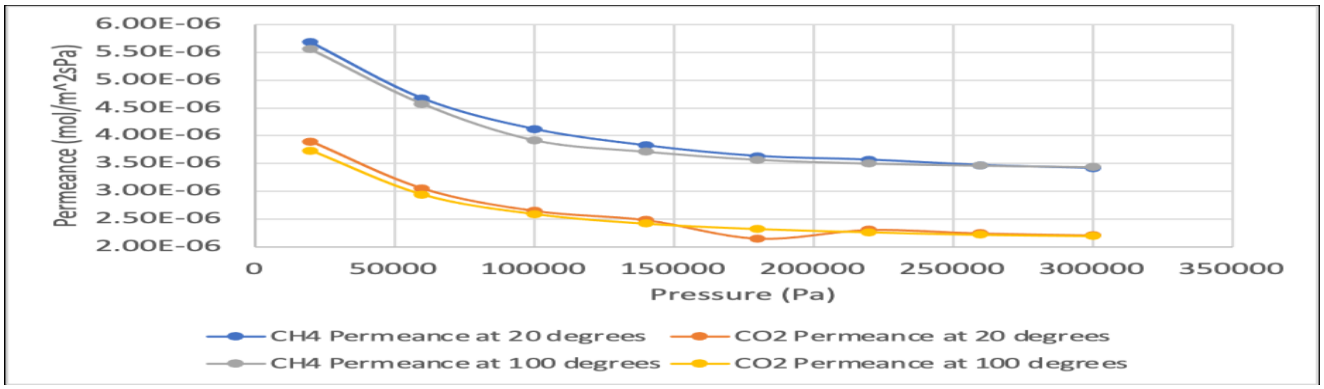

Figure 7. Effect of Pressure on Permeance using 15nm Membrane

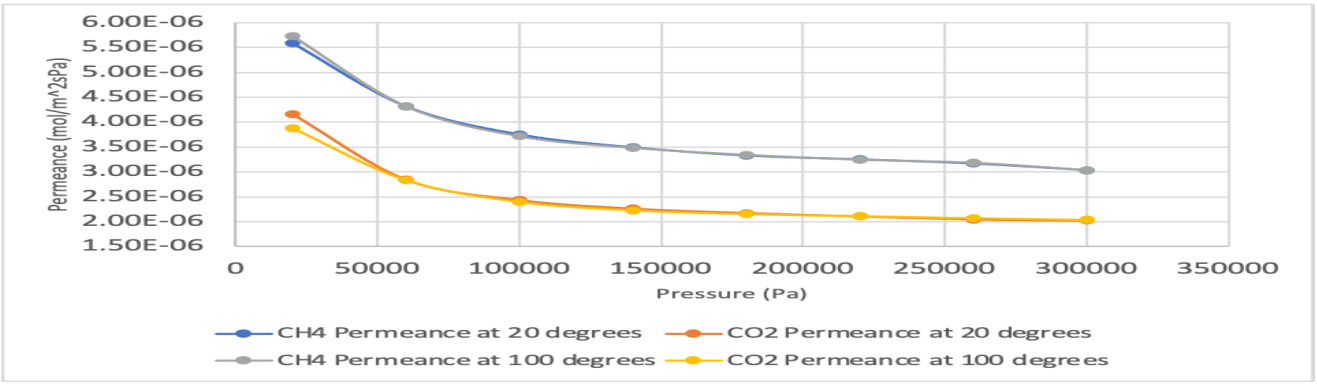

Figure 8. Effect of Pressure on Permeance using 200nm Membrane

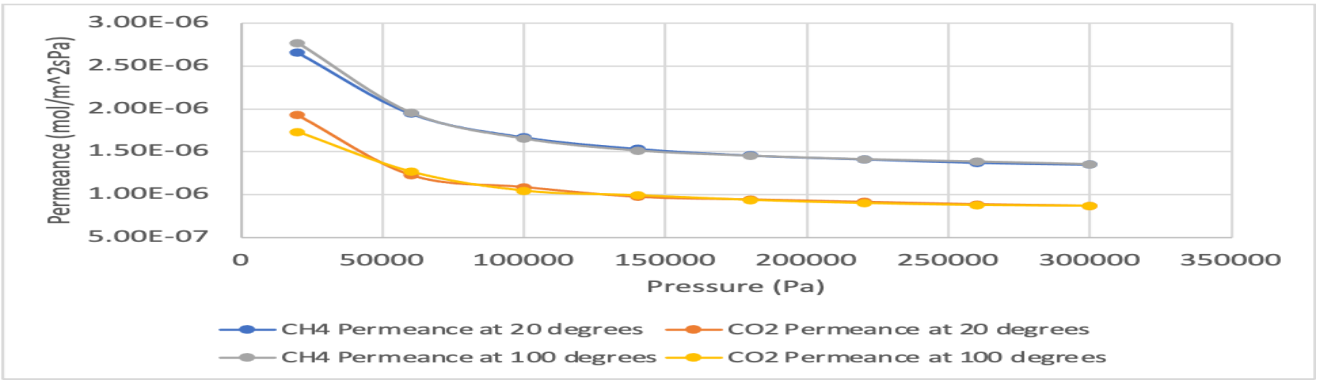

Figure 9. Effect of Pressure on Permeance using 6000nm Membrane

Variation of CO_2 and CH_4 Fluxes as a Function of Applied Trans-Membrane Pressure Drop

To understand how each transport mechanism varies with pressure change, we analyzed each of them separately as shown in Figure 10 and 11 by replotting the flux on the y-axis and trans-membrane pressure drop on the x-axis. As expected, results show that for each gas, temperature, and membrane there are three sections. In the first section up to the trans-membrane pressure drop of 60000 there is a linear variation of flux with trans-membrane pressure that passes through the origin ($0< \Delta P = 60000$pa). This is followed by a transition region where there is a bend (60000>TMP<100000) and then the third region where linearity does not pass through the origin ($\Delta P >100000$). The first region where the flux increases linearly with TMP passing through the origin is referred to as the viscous flow region. The variations of the fluxes versus applied pressure shows a linear increase in fluxes at low pressures passing through the origin (60000 Pa and below). However, when the operating pressure is over a critical value, there is the beginning of a deviation and relationship is no longer linear, which suggests that the flow regime is transitioning. As more pressure is applied the relationship is transferred from the Darcy

regime to the inertial flow regime where Darcy's law is not valid anymore. As shown in Figs. 10-11, at a higher pressure, there is linearity but does not extrapolate back to the origin which suggests that the inertial flow regime is dominant.

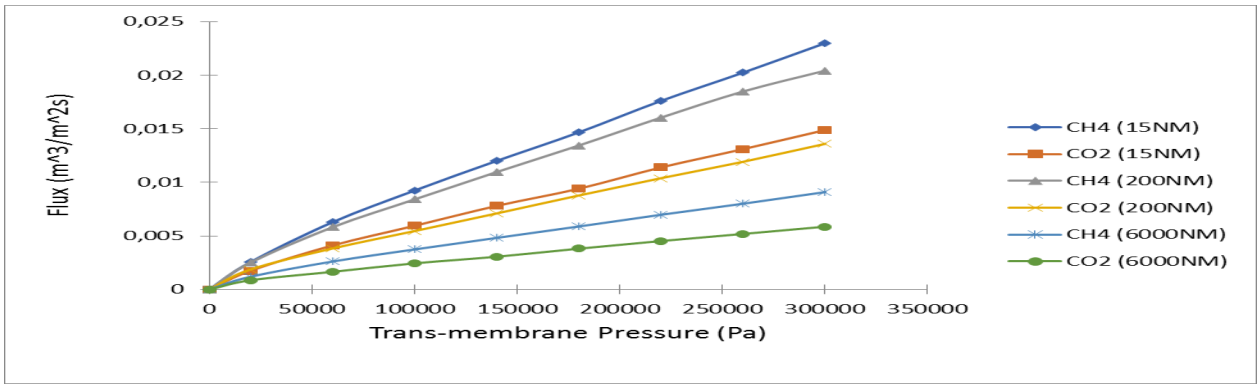

Figure 10. The Variation of CO_2 and CH_4 Fluxes for the Three Membranes studied as a Function of Applied Transmembrane Pressure for the Different Membranes at 20 Degrees C

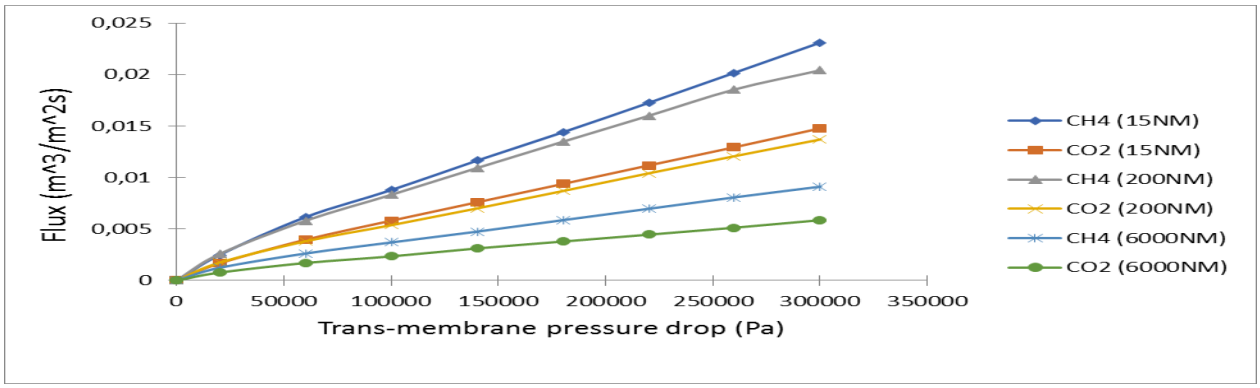

Figure 11. The Variation of CO_2 and CH_4 Fluxes for the Three Membranes studied as a Function of Applied Transmembrane Pressure for the Different Membranes at 100 Degrees C

Darcy Flow

Table 8 shows the gas flow regimes under different Knudsen number ranges. So, it is possible to also calculate the Knudsen number for gas flow in the membranes under different pore throat radius (PTR) and average pressure.

Table 8. Knudsen Number and Flow Regimes Classifications for Porous Media

Flow regime	Knudsen number	Model to be applied
Continuum (Viscous) flow	$K_n < 0.01$	Darcy's equation for laminar flow and Forchheimer's equation for turbulent flow
Slip flow	$0.01 < K_n < 0.1$	Darcy's equation with Klinkenberg or Knudsen's correction
Transition flow	$0.1 < K_n < 10$	Darcy's law with Knudsen's correction can be applied. alternative method is Burnett's equation with slip boundary conditions
Free molecular flow	$K_n > 10$	Knudsen's diffusion equation alternative methods are direct simulation Monte Carlo (DSMC) and lattice Boltzmann

The variation of CO_2 and CH_4 fluxes as a function of applied transmembrane pressure for the different membranes at 20 and 100 degrees C respectively was studied in the Darcy flow regime between a ΔP of 0 to 60000 Pa. Data for this evaluation are presented in Tables 9 - 14 and plotted in Figures 12 and 13 respectively.

Table 9. Darcy Regime Experimental Results for 15nm Pore Size Membrane at 20°C

Inlet Pressure (Pa)	CH_4 Outlet Flowrate at 20 degrees (LPM)	CO_2 Outlet Flowrate at 20 degrees (LPM)	CH_4 Outlet Flowrate at 20 degrees (m3/s)	CO_2Outlet Flowrate at 20 degrees (m3/s)	CH_4 Flux, Q_{CH4} (m3/m2/s)	CO_2 Flux, Q_{CH4} (m3/m2/s)
0.00000	0.00000	0.00000	0.00000	0.00000	0.00000	0.00000
20000	1.37	0.94	2.2833E-05	1.5667E-05	0.00254439	0.00174578
60000	3.38	2.21	5.6333E-05	3.6833E-05	0.00627739	0.00410445

Table 10. Darcy Regime Experimental Results for 200nm Pore Size Membrane at 20°C

Inlet Pressure (Pa)	CH_4 Outlet Flowrate at 20 degrees (LPM)	CO_2 Outlet Flowrate at 20 degrees (LPM)	CH_4 Outlet Flowrate at 20 degrees (m3/s)	CO_2 Outlet Flowrate at 20 degrees (m3/s)	CH_4 Flux, Q_{CH4} (m3/m2/s)	CO_2 Flux, Q_{CH4} (m3/m2/s)
0.00000	0.00000	0.00000	0.00000	0.00000	0.00000	0.00000
20000	1.57	1.17	2.6167E-05	0.0000195	0.00250399	0.00186603
60000	3.64	2.4	6.0667E-05	0.00004	0.00580542	0.00382775

Table 11. Darcy Regime Experimental Results for 6000nm Pore Size Membrane at 20°C

Inlet Pressure (Pa)	CH_4 Outlet Flowrate at 20 degrees (LPM)	CO_2 Outlet Flowrate at 20 degrees (LPM)	CH_4 Outlet Flowrate at 20 degrees (m3/s)	CO_2 Outlet Flowrate at 20 degrees (m3/s)	CH_4 Flux, Q_{CH4} (m3/m2/s)	CO_2 Flux, Q_{CO2} (m3/m2/s)
0.00000	0.00000	0.00000	0.00000	0.00000	0.00000	0.00000
20000	1.61	1.17	2.6833E-05	0.0000195	0.00118784	0.00086321
60000	3.54	2.24	0.000059	3.7333E-05	0.00261178	0.00165265

Table 12. Darcy Regime Experimental Results for 15nm Pore Size Membrane at 100°C

Inlet Pressure (Pa)	CH_4 Outlet Flowrate at 100 degrees (LPM)	CO_2 Outlet Flowrate at 100 degrees (LPM)	CH_4 Outlet Flowrate at 100 degrees (m3/s)	CO_2 Outlet Flowrate at 100 degrees (m3/s)	CH_4 Flux, Q_{CH4} (m3/m2/s)	CO_2 Flux, Q_{CO2} (m3/m2/s)
0.00000	0.00000	0.00000	0.00000	0.00000	0.00000	0.00000
20000	1.34	0.9	2.2333E-05	0.000015	0.00248867	0.0016715
60000	3.31	2.13	5.5167E-05	0.0000355	0.00614739	0.00395587

Table 13. Darcy Regime Experimental Results for 200nm Pore Size Membrane at 10 °C

Inlet Pressure (Pa)	CH_4 Outlet Flowrate at 20 degrees (LPM)	CO_2 Outlet Flowrate at 20 degrees (LPM)	CH_4 Outlet Flowrate at 100 degrees (m3/s)	CO_2 Outlet Flowrate at 100 degrees (m3/s)	CH_4 Flux, Q_{CH4} (m3/m2/s)	CO_2 Flux, Q_{CO2} (m3/m2/s)
0.00000	0.00000	0.00000	0.00000	0.00000	0.00000	0.00000
20000	1.61	1.09	2.6833E-05	1.8167E-05	0.00256778	0.00173844
60000	3.64	2.39	6.0667E-05	3.9833E-05	0.00580542	0.0038118

Table 14. Darcy Regime Experimental Results for 6000nm Pore Size Membrane at 100°C

Inlet Pressure (Pa)	CH4 Outlet Flowrate at 100 degrees (LPM)	CO_2 Outlet Flowrate at 100 degrees (LPM)	CH4 Outlet Flowrate at 100 degrees (m3/s)	CO_2 Outlet Flowrate at 100 degrees (m3/s)	CH4 Flux, Q_{CH4} (m3/m2/s)	CO_2 Flux, Q_{CO2} (m3/m2/s)
0.00000	0.00000	0.00000	0.00000	0.00000	0.00000	0.00000
20000	1.68	1.05	0.000028	0.0000175	0.00123949	0.00077468
60000	3.56	2.31	5.9333E-05	0.0000385	0.00262653	0.00170429

Darcy flow means that the velocity (v) of a fluid traveling through a porous medium is directly proportional to the pressure gradient, $\Delta P/\delta$ (a difference in pressure ΔP over some finite distance δ), and inversely proportional to the viscosity of the fluid or gas, μ. The flow of gas through a porous membrane is based on two concepts—transport mechanism e.g., Darcy flow through the porous medium and component material balance. In Darcy flow the proportionality constant κ, is called the permeability, and is used to characterize the porous medium. Thus, the Darcy formula for linear displacement is given by equation 4 (13).

$$q/A = Q = -\kappa\Delta P/\mu\delta \quad (4)$$

Where:

q =fluid volumetric flowrate, m^3s^{-1}
A = cross-sectional area of the porous medium perpendicular to the flow, m^2
Q = fluid Volume flux, $m^3\ m^{-2}s^{-1}$
κ = absolute permeability, m^2
ΔP = pressure difference (Pa) across the distance L parallel to the direction of flow, m
μ = the fluid viscosity, Pa-s
δ = finite distance, m

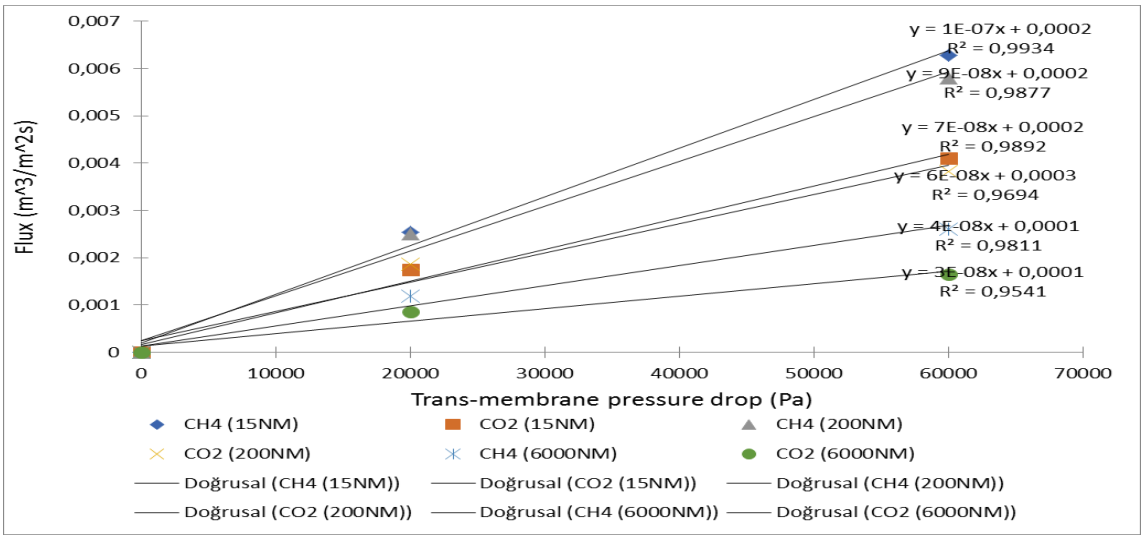

Figure 12. Flux Values as a Function of Trans-membrane Pressure for Each Gas and Membrane (20 degrees celsius) for Transmembrane Pressures from 6000Pa and below

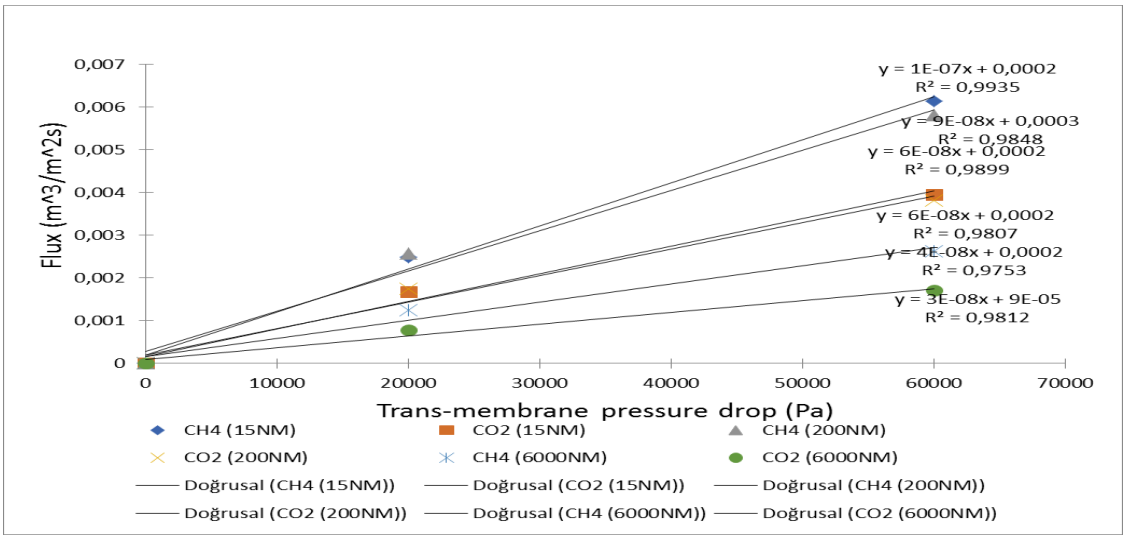

Figure 13. Flux Values as a Function of Trans-membrane Pressure for Each Gas and Membrane (100 degrees C) for 6000Pa and below

Mass Transfer Characteristics Through the Different Membranes and Effect of Pore Size and Porosity

The Reynolds number is dimensionless and comprises of the physical characteristics of the flow described by the ratio of inertial forces to viscous forces. It is a parameter convenient for predicting if a flow condition will be turbulent or laminar. Increasing Reynolds number is an indication of an increasing turbulent flow (Figure 14). It is defined as:

$$\mathrm{Re}_D = \frac{\rho VD}{\mu} = \frac{VD}{\nu} \tag{5}$$

and $\nu = \mu/\rho$ (6)

Where:
V = the flow velocity, m/s
D = characteristic linear dimension, m (travelled length of the fluid, hydraulic diameter etc.)
ρ = fluid density (kg/m^3),
μ = dynamic viscosity (Pa s),
ν = kinematic viscosity (m^2/s)

It can be interpreted that when viscous forces become dominant (slow flow, low Re) they are sufficient to keep all the fluid particles in line (Figure 14), then the flow is said to be laminar. Even incredibly low Re are an indication of viscous creeping motion, where the inertia effects are negligible. When the inertial forces dominate over the viscous forces (when the fluid is flowing faster and Re is larger) then the flow is said to turbulent (Figure 14).

Laminar Flow

For most practical purposes, if the Reynolds number is equal to or less than 2000, the flow is said to be laminar. In laminar flow, the viscous forces (forces of attraction) create more interaction between the layers and thus the mass transfer. Darcy law is applicable only on laminar flow, if we apply it in turbulent flow, we get errors in result. More pressure drop is required for the same or more flow rate, and as a result the direct linear relationship between and q and pressure drop deviate from linear behavior predicted in Darcy law. Laminar flow is characterised by:

- Re <= 2000
- 'low' velocity
- Fluid particles move in straight lines.
- Layers of flow over one another at different speeds with virtually no mixing between layers.
- The flow velocity profile for laminar flow in circular pipes is parabolic in shape, with a maximum flow at the centre of the pipe and a minimum flow at the pipe walls.
- The average flow velocity is approximately one half of the maximum velocity.
- Simple mathematical analysis is possible.

Transitional Flow

At Reynolds numbers increase between about 2000 and 4000 the flow is unstable due to the onset of turbulence. These flows are occasionally referred to as transitional flows. The accepted transition Reynolds number from laminar to turbulent flow in a circular pipe is $\mathrm{Re}_{D,crit} = 2300$.

Turbulent Flow

In turbulent flow random fluctuations occur with time in the magnitude of velocity components and an additional mechanism is present that causes the extra mass transfer and that is the formation of eddies. This is the sole reason why any transfer, be it heat, or mass is more in case of turbulent flow. This type of flow regime is characterised by:

- Re > 4000
- high' velocity
- irregularity in the movement of particles of the fluid.
- Average motion is in the direction of the flow.
- The flow velocity profile for turbulent flow is flat across the centre section of a pipe and drops rapidly extremely close to the walls.
- The average flow velocity is approximately equal to the velocity at the centre of the pipe.
- Mathematical analysis is exceedingly complex and difficult.

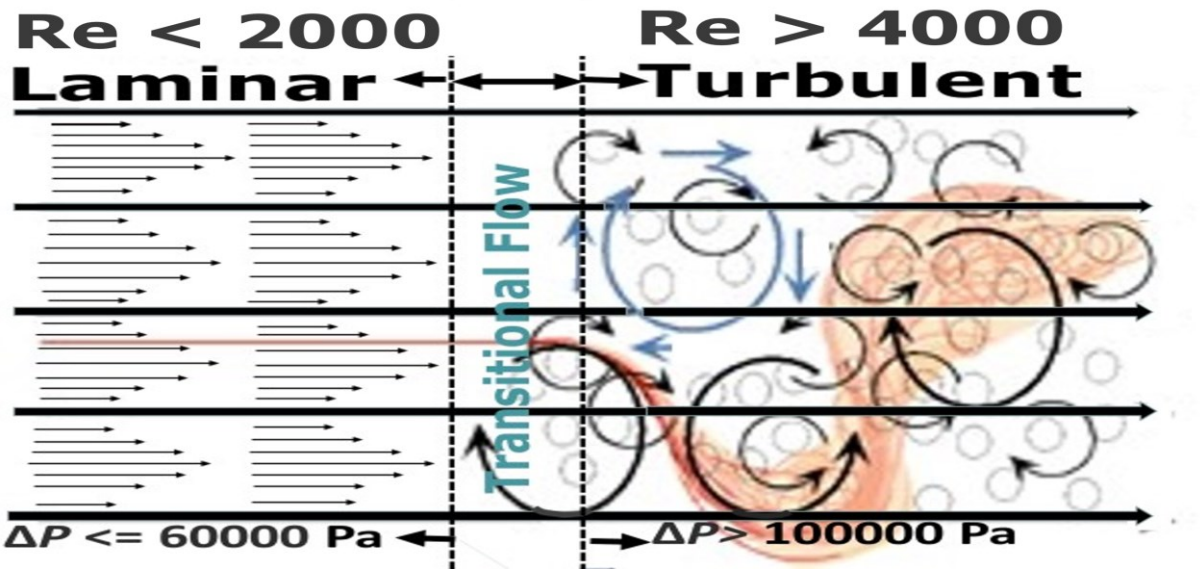

Figure 14. Turbulent and Laminar Flows

Darcy Parameters

To understand the mathematical aspect behind flow in the membrane substance, Darcy's law can be described as: Darcy's law describes the relationship among the instantaneous rate of discharge through porous medium and pressure drop at a distance. For transmembrane pressures equal to and less than or equal to 6000Pa equation 4 was applied from the plots of flux against trans-membrane pressure drop it was possible to calculate the Darcy permeability. These values are displayed in Tables 15 and 16 respectively for CO2 and CH4 for the three different membranes studied.

Table 15. Calculation of Darcy Permeability for CO_2

Membrane pore size (r_p), nm/Temperature, (°C)		δ, m	Slope = κ_i/μ_i δ, m/Pa-s	Darcy Permeability (κ) = Slope X μ_i δ, m^2
15	20 (°C)	10^-6	7*10^-8	1.0*10^-18
	100 (°C)	10^-6	6*10^-8	1.1*10^-18
200	20 (°C)	10^-3	6*10^-8	8.8*10^-16
	100 (°C)	10^-3	6*10^-8	1.1*10^-15
6000	20 (°C)	10^-3	3*10^-8	4.4*10^-16
	100 (°C)	10^-3	3*10^-8	5.6*10^-16

Table 16. Calculation of Darcy Permeability for CH_4

Membrane pore size (r_p), nm/Temperature, (°C)		δ, m	Slope = $\kappa_i/\mu_i L$, m/Pa-s	Darcy Permeability (κ) = Slope X $\mu_i\delta$, m^2
15	20 (°C)	10^-6	1*10^-7	1.1*10^-18
	100 (°C)	10^-6	1*10^-7	1.4*10^-18
200	20 (°C)	10^-3	9*10^-8	9.9*10^-16
	100 (°C)	10^-3	9*10^-8	1.2*10^-15
6000	20 (°C)	10^-3	4*10^-8	4.4*10^-16
	100 (°C)	10^-3	4*10^-8	5.4*10^-16

Parameters for Integration

A schematic of the flow within a single membrane tube in a sheel and tube arrangement is presented in Figure 15. Flow enters from the top and passes through the permeable walls. Beyond the capped end, the fluid continues to an outlet following the black arrows. The inside of the membrane-walled channel is referred to as Region 1, while that outside is Region 2.

In all filtration scenarios, the main quantity of interest is the volumetric flux across the porous wall, which depends on the local transmembrane pressure, ΔP: the more spatially uniform the ΔP, the more effectively the membrane area is used for filtration. The ΔP is a complex function of operating flux, membrane wall permeability and, crucially, the packing density of the membrane tubes within a device. Hurwitz [14] modelled the direct-flow process by considering the flow inside a single porous tube with a capped end. The flow was solved for in the asymptotic limits of low permeability and low Reynolds number. In both Hurwitz (14) and Sanaei et al. (15), the coupling that results from the flow on the permeate side was not considered. Griffiths et al. (16) address the question of how to choose the spatial dependence of the wall permeability to allow for the uniform delivery of solute (nutrient) across the permeable wall in a crossflow device.

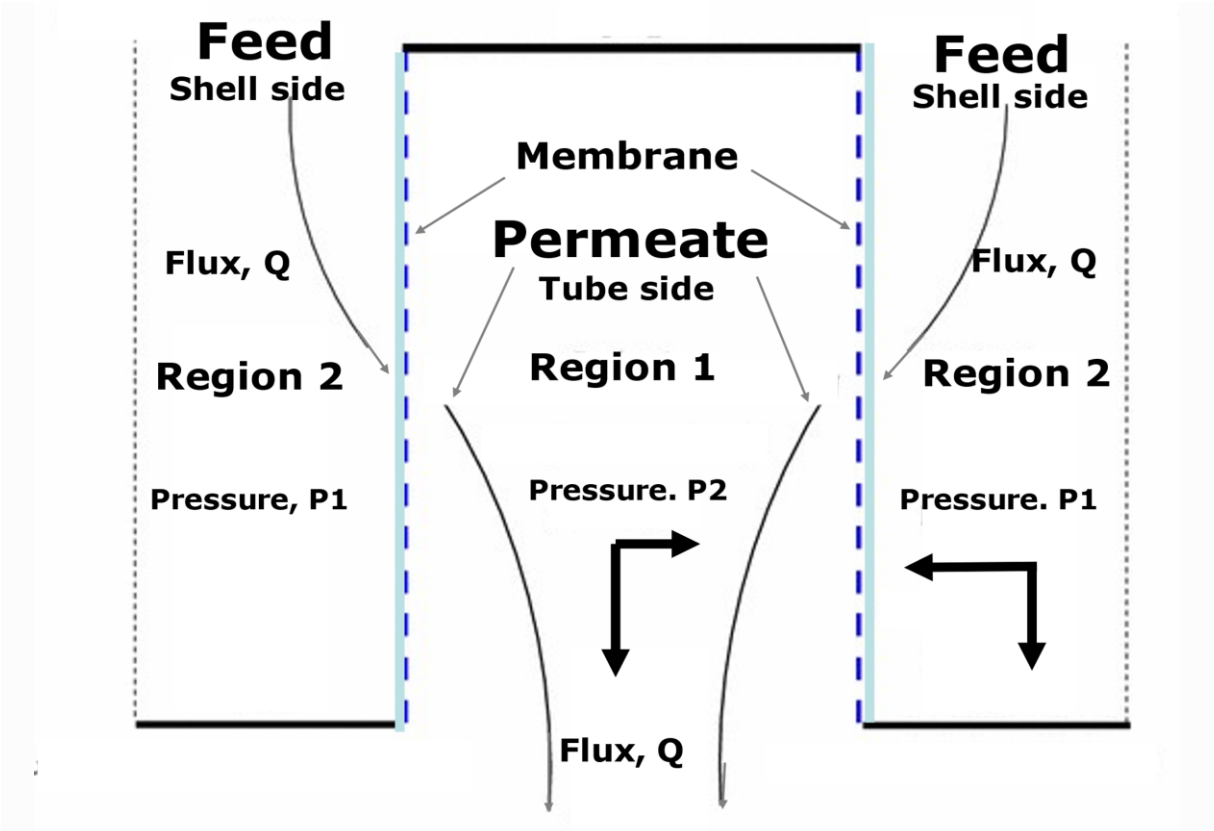

Figure 15. Schematic of the Flow within the Shell (Region 2) and tube (Region 1) with the Solid Lines indicating impermeable walls, the blue dashed lines indicating permeable walls, and the dotted line indicating the stainless-steel outer shell on which the heating jacket is mounted

Governing Equations and Parameters for Integration

Figure 16 shows a schematic Illustration of the membrane flow geometry. It consists of a tubular channel surrounded by a porous membrane. The CH4 and CO2 is treated as Newtonian and incompressible fluid with uniform physical properties. The flow is axisymmetric and isothermal, and the total density of the mixture is constant. The diffusion coefficient is assumed to be independent of the concentration. The permeability of the porous layer is constant, and the parabolic velocity distribution is considered at the inlet through the porous layer. The parabolic inlet profile is assumed to be continuous in the membrane with continuous derivatives. The membrane selectivity and permeability are taken as constant. Also, the porous membrane is assumed to be saturated since pure components are used. Fluid enters the shell side (Region 1) at a fixed flux Q which passes through the membrane side walls, and into the tube side permeate region (Region 2). Since the membrane tube is not in a bundle with other tubes it is considered an isolated channel

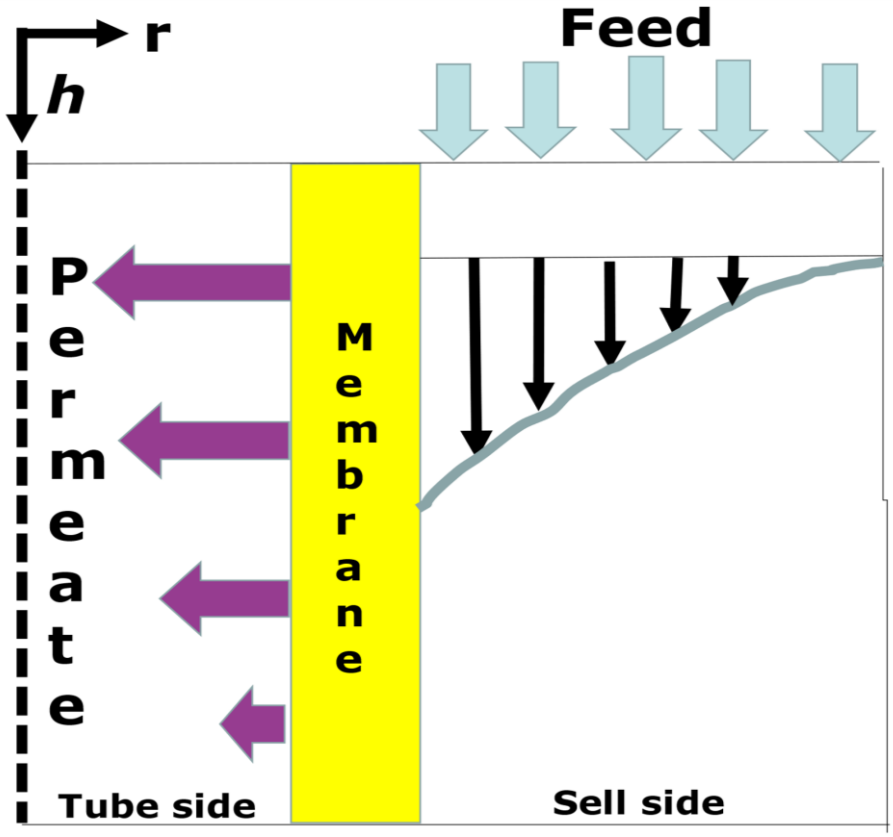

Figure 16. Schematic Illustration of the Membrane Flow Geometry

Figure 17 is section of membrane tube showing parameters for integration. On the other hand, gas transport through a porous tubular membrane can also be due to the viscous flow in the parallel pores, and the steady-state gas volume flux q (m3 /s) in these pores can also be estimated from Darcy's law (17)

$$q_i = \kappa_i (dp_i/dr)/\mu_i \quad (7)$$

where:
μi is the gas viscosity, Pa s
κi is permeability of the membrane, for gas I, m^2

Since our flux is in the radial direction (tubular membrane) the surface area A (m^2) is calculated by:

$$A = 2\pi rL \quad (8)$$

Where:
L = the length of the membrane, m
r = the membrane outer radius, m

Therefore equation 7 can be written as

$$q_i/2\pi rL = -[\kappa_i/\mu_i]dp_i/dr \quad (9)$$

$$dp_i = (q_i\mu_i/2\pi\kappa_i L)dr/r \quad (10)$$

Integrating, we get that

$$\int_{Pw}^{Pe} dp_i = \int_{rw}^{re}[(q_i\mu_i/2\pi\kappa_i L)]dr/r \quad (11)$$

$$Pe_i - Pw_i = [(q_i\mu/2\pi\kappa_i L)]\ln[re/rw] \quad (12)$$

$$q_i = 2\pi\kappa_i L(Pe_i - Pw_i)/\mu_i \ln[re/rw] \quad (13)$$

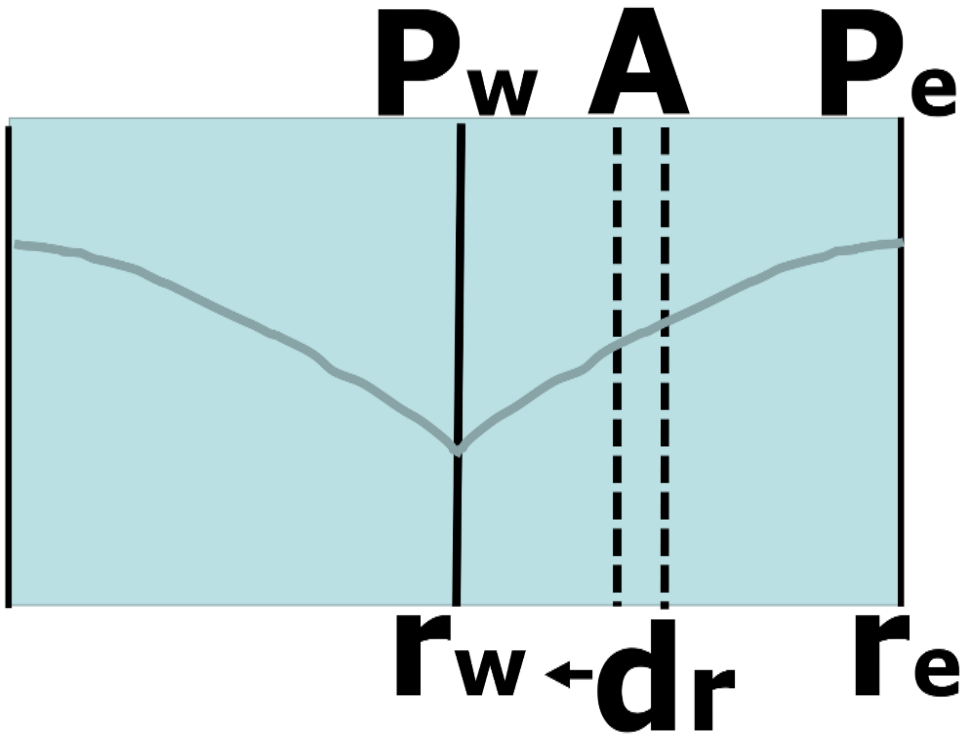

Figure 17. Section of Membrane Tube showing Parameters for integration

The Darcy permeability κ_i for component i has been obtained experimentally by varying qi through the membrane, the pressure drop across the membrane is recorded and plotted and from the slope κ is calculated. The formula of Darcy to meter squared (m2), is 1 Darcy is equivalent to 9.869E-13 meter squared (m2).

Table 17. Calculation of Darcy Permeability for CO_2 using radial flow

Membrane pore size (r_p), nm/Temperature		In[re/rw]	Slope = $2\pi\kappa_{ii}L/\mu_i\ln[re/rw]$, m^3/Pa-s	Darcy Permeability (κ_i) = Slope X $\mu_i\ln[re/rw]/2\pi L$, m^2
15	20 (°C)	0.3531	$7*10^{-8}$	$1.7*10^{-13}$
	100 (°C)	0.3531	$6*10^{-8}$	$1.9*10^{-13}$
200	20 (°C)	0.3180	$6*10^{-8}$	$1.4*10^{-13}$
	100 (°C)	0.3180	$6*10^{-8}$	$1.7*10^{-13}$
6000	20 (°C)	0.2224	$3*10^{-8}$	$4.9*10^{-14}$
	100 (°C)	0.2224	$3*10^{-8}$	$6.1*10^{-14}$

Table 18. Calculation of Darcy Permeability for CH_4 using Radial Flow

Membrane pore size (r_p), nm/Temperature		In[re/rw]	Slope = $2\pi_i L/\mu_i \ln[re/rw]$ m^3/Pa-s	Darcy Permeability (κ_i) = Slope X $\mu_i \ln[re/rw]/2\pi L$, m^2
15	20 (°C)	0.3531	$1*10^{-7}$	$1.8*10^{-13}$
	100 (°C)	0.3531	$1*10^{-7}$	$2.2*10^{-13}$
200	20 (°C)	0.3180	$9*10^{-8}$	$1.5*10^{-13}$
	100 (°C)	0.3180	$9*10^{-8}$	$1.9*10^{-13}$
6000	20 (°C)	0.2224	$4*110^{-8}$	$4.9*10^{-14}$
	100 (°C)	0.2224	4*10^-8	$6.0*110^{-14}$

Comparison of Achieved Gas Removal Rates in Porous Membrane Systems Used in this Study Compared with Dense Membrane Systems

Figure 18 shows the description of external mass transfer rates are changing with the gas stream velocity and Table 19 presents the membrane dimensions. In these experiments, increases in contact times were achieved by decreasing the flow rate of the feed gas mixture while maintaining a constant catalyst charge. Operation under such conditions means that the external mass transfer rates are changing with the gas stream velocity.

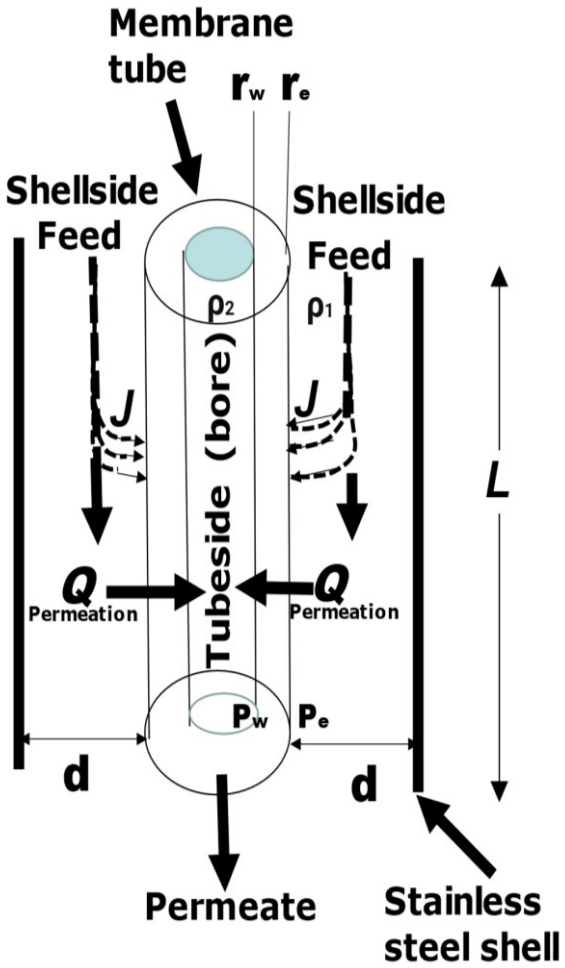

Figure 18. Description of External Mass Transfer Rates are Changing with the Gas Stream Velocity

Table19. Membrane Dimensions

Membrane	OD, mm	ID, mm	OD – ID, mm	(OD – ID)/2 = d, mm	Permeation Length, h, mm
15nm	10.03	7.05	2.98	1.49	338
200nm	10.5	7.64	2.86	1.43	330
6000nm	25.07	20.07	5.0	2.5	320

The impact of such changes upon the permeation rate was evaluated by calculating the gas mass transfer flux J_I, to the membrane inner surface as described in Figure 18 and is is given by eq. (14).

$J_i = (\rho_1 — \rho)Sh\ Dei/d)$ (14).

Where:
ρ_1 = molar gas density on the shell side, gmol/cm3
ρ_2 = molar gas density on the permeate side, gmol/cm3
De = the diffusivity of gas in the shell-side (cm2/s);
d = the annular diameter (cm)
Sh = the Sherwood number.

The value of De was estimated as indicated above [eq. (16)]. The gas molar density of the gas ρ is giving by:

$\rho = PM/RT\ (atm)\ (g/mol)/[L\ atm/mol\ K](K)$ (15)

Where:
P = the pressure, atm
M = the molecular weight, g/mole
R = the gas constant, $L{\cdot}atm{\cdot}K^{-1}{\cdot}mol^{-1}$
T = the absolute temperature, K

Across the PDMS membrane, gas transport is due to solution and diffusion, and the steady-state gas mass flux N (kg/m2 /s) obeys the equation (18)

$N = P\Delta p/h$ (16)

Where:
h = the membrane thickness,
Δp = the pressure difference across the membrane
P = the gas permeability, which is 1.34x10-16 kmol/(Pa s m2) for Nitrogen.

On the other hand, gas transport through a porous membrane, is due to the viscous flow in the parallel pores, and the steady-state gas volume flux q (m3 /m2 /s) can be estimated from Darcy's law (17):

Table 20. Permeability of Dense PDMS Membrane

Gas	Permeance, kmol/m^2Pa-s	Molecular Weight, Kg/Kmol	PDMS Mass Flux, N (kg/m^2Pa-s)	PDMS Mass Flux, N (g/cm^2Pa-s)	PDMS Mass Flux, N (g/cm^2s)	
					20000 Pa	60000 Pa
N2	1.34x10^-16	28.0	37.52 x10^-16	37.52 x10^-17	7.564.32 x10^-12	22.564.32 x10^-12
CO2	12.73X10^-16	44.0	558.12 x10^-16	558.12 x10^-17	111.664.32 x10^-12	334.8764.32 x10^-12
CH4	4.02 X 10^-16	16.0	64.32 x10^-16	64.32 x10^-17	12.864.32 x10^-12	38.5964.32 x10^-12

$q/A = \kappa\Delta p/\mu h$ (16)

where:
μ = the gas viscosity,
κ = permeability of the membrane, which has been obtained experimentally as follows.
H = arbitrary length

By varying the airflow q through the membrane, the pressure drop across the membrane is recorded and plotted. For fluid Reynolds numbers in the range 1 to 4000 and flow of a fluid at right angles to the cylindrical structure, the averaged mass transfer coefficient around the periphery is given by:

$\underline{S}h = 1.86(ReD)^{0.33}(Sc)^{0.33}$ (17)

Where:
Re = Reynolds number
Sc = Schmidt number

The Schmidt number is obtained from eq. (18).

$Sc = \mu/\rho\ De$ (18)

Where:
μ = the viscosity of gas, Pa s
ρ = density of the gas, Kg/m^3

The Reynolds number is obtained from eq. (24)

$$Re_D = \frac{\rho VD}{\mu} = \frac{VD}{\nu} \quad (19)$$

Where:
V = the superficial fluid velocity, m/s
D = the characteristic distance, m
ρ = the fluid density, Kg/m^3
ν = the kinematic viscosity (which can be acquired from data tables), m^2/s
μ = the dynamic viscosity (which can be acquired from data tables), Pa s

Table 21. Units of Dynamic and Kinematic Viscosity

Dynamic Viscosity		Kinematic Viscosity	
Unit	**Equivalent**	**Unit**	**Equivalent**
1 mPa-s	1 cP	1 cm^2/s	100 cSt
1 P (*Poise*)	100 cP	1 St	100 cSt
1 Pa-s	1000 cP	1 m^2/s	1,000,000 cSt

Haven established that the flow is laminar and confirmed by adherence to Darcy Law as shown in the high correlation coefficients observed in Figures 12 and 13, means that the Reynolds number is 2000 and lower. We can therefore select any value of Reynolds number from 2000 and below. We used values of 1, 1000 and 2000 to calculate the $\underline{S}_h$ and subsequently J_i. This enables calculation of V, the superficial fluid velocity. The Sherwood number is a better indicator of the membrane performance since it eliminates the effects of the concentration conditions at the inlet and the length of the test section. The Sherwood number is predicted using both Darcy's law.

Table 22. Gas Mass Transfer Flux from the Bulk Gas in the Shell-side to the Membrane Outer Surface

MEMBRANE	(ρ1--ρ2)Dei/d		$\underline{S}h$		Re		Sc (10^-6)		Gas mass transfer flux from the bulk gas in the shell-side to the membrane outer surface, $J_{CH4}(g/cm^2\ s)$	
Pore Size (nm)	20 (°C)	100 (°C)	20 (°C)	100 (°C)	20 (°C)	100 (°C)	20 (°C)	100 (°C)	20 (°C)	100 (°C)
15	0.0589	0.0708	0.0362 – 0.4451	0.0365 – 0.4482	<=2000	<=2000	6.56	6.70	2.13x10^-3 – 0.0262	2.58x10^-3 – 0.0317
200	0.0621	0.0746	0.0362 – 0.4451	0.0365 – 0.4482	<=2000	<=2000	6.56	6.70	2.25x10^-3 – 0.0276	2.72x10^-3 – 0.0334
6000	0.0189	0.0228	0.0362 – 0.4451	0.0365 – 0.4482	<=2000	<=2000	6.56	6.70	6.84x10^-4 – 8.41x10^-3	8.32x10^-4 – 0.0102

Table 23. Superficial Velocity for CH4 at 20°C, m/s

CH4 20oC	Reynolds Number (ReD)	Superficial Velocity (V), m/s
15nm	1	3.49X10^-9
	1000	3.49X10^-6
	2000	6.97X10^-6
200nm	1	3.67X10^-9
	1000	3.67X10^-6
	2000	7.35X10^-6
6000nm	1	1.12X10^-9
	1000	1.12X10^-6
	2000	2.25X10^-6

Table 24. Superficial Velocity for CH4 at 100oC, m/s

CH4 100oC	Reynolds Number (ReD)	Superficial Velocity (V), m/s
15nm	1	5.45X10^-9
	1000	5.45X10^-6
	2000	1.09x10^-5
200nm	1	5.74X10^-9
	1000	5.74X10^-6
	2000	1.15x10^-5
6000nm	1	1.75X10^-9
	1000	1.75X10^-6
	2000	3.51X10^-6

Table 25. Superficial Velocity for CO2 at 20oC, m/s

CO2 20oC	Reynolds Number (ReD)	Superficial Velocity (V), m/s
15nm	1	1.69X10^-9
	1000	1.69X10^-6
	2000	3.39X10^-6
200nm	1	1.79X10^-9
	1000	1.79X10^-6
	2000	3.57X10^-6
6000nm	1	5.46X10^-10
	1000	5.46X10^-7
	2000	1.09X10^-6

Table 26. Superficial Velocity for CO2 at 20oC, m/s

CO2 100oC	Reynolds Number (ReD)	Superficial Velocity (V), m/s
15nm	1	2.72X10^-9
	1000	2.72X10^-6
	2000	5.43X10^-6
200nm	1	2.86X10^-9
	1000	2.86X10^-9
	2000	5.72X10^-6
6000nm	1	8.74X10^-10
	1000	8.74X10^-7
	2000	1.75X10^-6

Using equations (14-17) the gas mass transfer flux from the bulk gas in the shell-side to the membrane outer surface J was calculated for CO2 and CH4 and are presented in Tables 27 and 28 respectively.

Table 27. Comparison of Achieved Gas Removal Rates in Porous Membrane Systems used in in This Study compared with Dense Membrane Systems for $_i$ = CH4 = 0.6BARRER)

Membrane	(ρ1--ρ2)Dei/		Sh		Re		Sc X10^-6		Gas mass transfer flux from the bulk gas in the shell-side to the membrane outer surface, J_{CH4} (g/cm^2 s)	
Pore Size (nm)	20 (°C)	100 (°C)	20 (°C)	100 (°C)	20 (°C)	100 (°C)	20 (°C)	100 (°C)	20 (°C)	100 (°C)
15	0.1769	0.2124	0.0329 - 0.4048	0.0332 – 0.4077	<=2000	<=2000	4.92	5.03	5.82X10^-3 – 0.0716	7.05x10^-3 – 0.0866
200	0.1863	0.2237	0.0329 - 0.4048	0.0332 – 0.4077	<=2000	<=2000	4.92	5.03	6.13x10^-3 – 0.0754	7.43x10^-3 – 0.0912
6000	0.0569	0.0684	0.0329 - 0.4048	0.0332 – 0.4077	<=2000	<=2000	4.92	5.03	1.87x10^-3 – 0.0230	2.27x10^-3 – 0.0279

Table 28. Comparison of Achieved Gas Removal Rates in Porous Membrane Systems used in in This Study for $_i$ = CO2 = 0.2BARRER)

Membrane	ρ1-- ρ2) Dei/d		Sh		Re		Sc X10^-6		Gas mass transfer flux from the bulk gas in the shell-side to the membrane outer surface, J_{CH4} (g/cm^2 s)	
Pore Size (nm)	20 (°C)	100 (°C)	20 (°C)	100 (°C)	20 (°C)	100 (°C)	20 (°C)	100 (°C)	20 (°C)	100 (°C)
15	0.1235	0.1528	0.0312 – 0.3836	0.0314 – 0.3859	<=2000	<=2000	4.18	4.26	3.85x10^-3 – 0.0474	4.79x10^-3 – 0.0589
200	0.1301	0.1610	0.0312 – 0.3836	0.0314 – 0.3859	<=2000	<=2000	4.18	4.26	4.06x10^-3 – 0.0499	5.06x10^-3 – 0.0621
6000	0.0398	0.0492	0.0312 – 0.3836	0.0314 – 0.3859	<=2000	<=2000	4.18	4.26	1.24x10^-3 – 0.0153	1.54x10^-3 – 0.0189

Table 29. Comparison of Achieved Gas Removal Rates in Porous Membrane Systems used in in This Study for $_i$ = CO2 = 0.6 BARRER)

Membrane	(ρ1-- ρ2)Dei/d		Sh		Re		Sc X10^-6		Gas mass transfer flux from the bulk gas in the shell-side to the membrane outer surface, J_{CH4}(g/cm^2 s)	
Pore Size (nm)	20 (°C)	100 (°C)	20 (°C)	100 (°C)	20 (°C)	100 (°C)	20 (°C)	100 (°C)	20 (°C)	100 (°C)
15	0.3706	0.4585	0.0284 – 0.3490	0.0286 – 0.3508	<=2000	<=2000	3.14	3.19	0.0105 – 0.1293	0.0131 – 0.1608
200	0.3904	0.4830	0.0284 – 0.3490	0.0286 – 0.3508	<=2000	<=2000	3.14	3.19	0.0111– 0.1362	0.0138 – 0.1694
6000	0.1193	0.1477	0.0284 – 0.3490	0.0286 – 0.3508	<=2000	<=2000	3.14	3.19	3.39x10^-3 – 0.0416	4.22x10^-3 – 0.0518

Using equations 14-17, the gas mass transfer flux from the bulk gas in the shell-side to the membrane outer surface J. We used Re of 1, 1000 and 2000 to calculate the range for J. It is very unlikely that a Re value as low as 1 would be of any significant practical application in membrane separation and therefore Re values closer to 2000 are more realistic. As shown in Tables 30-33 J values obtained for Re = 2000 were found to be always greater than the permeation flux Q, and therefore, although the gas stream velocity changes the rates of transfer of gas to the membrane surface are sufficient to sustain its permeation through the membrane for the two transmembrane pressure drops and temperatures studied. Darcy's law can be extended with a nonlinear term are used to simulate the flow in the lumen. The percentage mass predicted using both models can then be compared. There is no discernible difference between the predicted percentage mass change of CH4 and CO2; implying that the linear relationship between the velocity and the pressure gradient is accurate enough. For higher permeability of the porous medium, the nonlinear terms and the inertial effects can be important. Percentage mass change of both species decreases sharply with an increase of flow rate. This is since the residence time of the mixture gets shorter as the flow rate is increased.

According to Figure 12 and 13 κ is calculated and displayed in Tables 30-33 for membranes with 15nm, 200nm and 6000nm pores respectively. Calculations in Tables 30-33 reveals that, under the same pressure drop across the membrane, the mass/volume flux in porous membrane can be over four orders of magnitude higher than in a PDMS membrane with the similar thickness. Such extraction rate is four orders of magnitude greater than previously reported using a PDMS membrane (18). This enhancement is probably due to the different gas transport mechanisms.

Table 30. Comparison of Achieved Gas Removal Rates in Porous Membrane Systems used in in This Study Compared with Dense Membrane Systems for $_i$ = CH4 = 0.2 BAR)

Membrane pore size (r_p), nm	Thickness h (μm)	Permeability, κ (m^2)		Pressure drop across membrane Δp (kPa)		Mass flux (N_{CH4} (kg/m^2 s)	Volume flux Q_{CH4} (g/cm^2 s)		Gas mass transfer flux from the bulk gas in the shell-side to the membrane outer surface, J_{CH4} (g/cm^2 s)	
		20 (°C)	100 (°C)	20 (°C)	100 (°C)	35 (°C)	20 (°C)	100 (°C)	20 (°C)	100 (°C)
15	10^{-6}	1.8*10^{-13}	2.2*10^{-13}	60	60	12.864x10^-12	1.69x10^-4	1.30x10^-4	2.13x10^-3 – 0.0262	2.58x10^-3 – 0.0317
200	10^{-3}	1.5*10^{-13}	1.9*10^{-13}	60	60	12.864x10^-12	1.66x10^-4	1.34x10^-4	2.25x10^-3 – 0.0276	2.72x10^-3 – 0.0334
6000	10^{-3}	4.9*110^{-14}	6.0*10^{-14}	60	60	12.864x10^-12	7.92x10^-5	6.48x10^-5	6.84x10^-4 – 8.41x10^-3	8.32x10^-4 – 0.0102

Table 31. Comparison of Achieved Gas Removal Rates in Porous Membrane Systems used in in This Study Compared with Dense Membrane Systems for $_i$ = CH4 = 0.6 BAR

Membrane pore size (r_p), nm	Thickness h (μm)	Permeability, κ (m^2)		Pressure drop across membrane Δp (kPa)		Mass flux N_{CO2} ($kg/m^2/s$)	Volume flux Q_{CH4} (g/cm^2s)		Gas mass transfer flux from the bulk gas in the shell-side to the membrane outer surface, J_{CO2} (g/cm^2s)	
		20 (°C)	100 (°C)	20 (°C)	100 (°C)	35 (°C)	20 (°C)	100 (°C)	20 (°C)	100 (°C)
15	10^{-6}	$1.8*10^{-13}$	$2.2*10^{-13}$	60	60	38.5964.32 x10^-12	4.17 x10^ -4	3.21x10 ^-4	5.82X10^-3 – 0.0716	7.05x10^-3 – 0.0866
200	10^{-3}	$1.5*10^{-13}$	$1.9*10^{-13}$	60	60	38.5964.32 x10^-12	3.87 x10^ -4	3.04x10 ^-4	6.13x10^-3 – 0.0754	7.43x10^-3 – 0.0912
6000	10^{-3}	$4.9*10^{-14}$	$6.1*10^{-14}$	60	60	38.5964.32 x10^-12	1.74 x10^ -4	1.37x10 ^-4	1.87x10^-3 – 0.0230	2.27x10^-3 – 0.0279

Table 32. Comparison of Achieved Gas Removal Rates in Porous Membrane Systems used in in This Study Compared with Dense Membrane Systems for $_i$ = C02= 0.2 BARRER)

Membrane pore size (r_p), nm	Thickness h (μm)	Permeability, κ (m^2)		Pressure drop across membrane Δp (kPa)		Mass flux (N_{CH4} (kg/m^2 s)	Volume flux Q_{CO2} (g/cm^2 s)		Gas mass transfer flux from the bulk gas in the shell-side to the membrane outer surface, J_{CH4} (g/cm^2 s)	
		20 (°C)	100 (°C)	20 (°C)	100 (°C)	35 (°C)	20 (°C)	100 (°C)	20 (°C)	100 (°C)
15	10^{-6}	$1.8*10^{-13}$	$2.2*10^{-13}$	60	60	111.664x10-12	3.20x10^-4	2.40x10^-4	3.85x10^-3 – 0.0474	4.79x10^-3 – 0.0589
200	10^{-3}	$1.5*10^{-13}$	$1.9*10^{-13}$	60	60	111.664x10-12	3.40x10^-4	2.49x10^-4	4.06x10^-3 – 0.0499	5.06x10^-3 – 0.0621
6000	10^{-3}	$4.9*10^{-14}$	$6.0*10^{-14}$	60	60	111.664x10-12	1.58x10^-4	1.11x10^-4	1.24x10^-3 – 0.0153	1.54x10^-3 – 0.0189

Table 33. Comparison of Achieved Gas Removal Rates in Porous Membrane Systems used in in This Study Compared with Dense Membrane Systems for $_i$ = CO2 = 0.6 BARRER)

Membrane pore size (r_p), nm	Thickness h (μm)	Permeability, κ (m^2)		Pressure drop across membrane Δp (kPa)		Mass flux N_{CO2} ($kg/m^2/s$)	Volume flux Q_{CO2} (m^3/m^2s)		Gas mass transfer flux from the bulk gas in the shell-side to the membrane outer surface, J_{CO2} (g/cm^2s)	
		20 (°C)	100 (°C)	20 (°C)	100 (°C)	35 (°C)	20 (°C)	100 (°C)	20 (°C)	100 (°C)
15	10^{-6}	$1.8*10^{-13}$	$2.2*10^{-13}$	60	60	334.8764.32 x10-12	7.50x10^-4	5.69x10^-4	0.0105 – 0.1293	0.0131 – 0.1608
200	10^{-3}	$1.5*10^{-13}$	$1.9*10^{-13}$	60	60	334.8764.32 x10-12	7.01x10^-4	5.48x10^-4	0.0111– 0.1362	0.0138 – 0.1694
6000	10^{-3}	$4.9*110^{-14}$	$6.1*10^{-14}$	60	60	334.8764.32 x10-12	3.02x10^-4	2.44x10^-4	3.39x10^-3 – 0.0416	4.22x10^-3 – 0.0518

Conclusion and Future Work

We have demonstrated and explained a relatively simple but effective way to estimate mass transfer from bulk gas to the membrane surface and compare that with the permeation rate by integrating porous membranes with different porosities and pore sizes. We have also compared the performance of our porous systems with that of a classical dense membrane composed of a transparent polymer with the ability to completely filter gas rates up to

7.4 micro litres/s/mm^2 of membrane area and our porous systems have shown that the dense system is limited by the low permeability although it possesses high selectivity. The device used involves a mass transfer section on the shell side, permeation through the membrane and a gas removal section on the tube side (bore). In the annular space section (Region 1), a high mass transfer is established generating the strong concentration gradient for gas transfer onto the membrane surface which is then subsequently transported across the membrane structure where the constituent slide along membrane until complete removal from the tube side and metered. The system has been successfully modeled based on Darcy's Law, and four necessary operating criteria have been determined to achieve a complete mass transfer of the gas from the shell side. The first criterion is that the various transport mechanisms occur in parallel. The second criterion is that at lower ΔP Darcy Law is applicable. The third criterion is that the gas mass transfer rates from the bulk stream in the shell side to the membrane surface is by far higher than a critical value of the permeation rate through the membrane: otherwise, gas is not able to flow through the membrane at economic rates and the membrane prevents mass transfer. The fourth criterion is that the ΔP across the membrane should not be larger than a critical pressure value otherwise any additional pressure is wasted.

Acknowledgement

The authors would like to thank Robert Gordon University for the use of its facility to complete the work. This study was funded by the TETFUND, PTDF and NDDC respectively

References

1. Ekinci, K. L., Yakhot, V. & Rajauria, S. (2010) High-frequency nanofluidics: A universal formulation of the fluid dynamics of MEMS and NEMS. Lab on A Chip.1 10(22) pp3013-25.doi: 10.1039/c003770m
2. Chua, Y. T., Ji, G. & Birkett, G. (2015) Nanoporous organosilica membrane for water desalination: Theoretical study on the water transport. Journal of Membrane Science. 482, pp56–66.
3. Ou, C., Rui, R. & Li, C. (2016) Multi-index and two-level evaluation of shale gas reserve quality. Journal of Natural Gas Science and Engineering.35, pp1139–1145.
4. Fan, D. & Ettehadtavakkol (2016) A. Transient shale gas flow model. Journal of Natural Gas Science and Engineering. 33, pp1353–1363.
5. Ceramic membranes - Guo Chu Technology (http://www.guochukeji.com/en/bzsb/moyuanjian/4312.html?msclkid=055f5fb2c080199594a73e2bd6831f90)
6. E.-U. Schlünder, J. Yang and A. Seidel-Morgenstern (2006) Competitive diffusion and adsorption in Vycor glass membranes—A lumped parameter approach, Catalysis Today 118(1-2) pp113-120, DOI:10.1016/j.cattod.2005.11.094)
7. Chen, X., Fan, Y., Wu, L. et al. (2021) Ultra-selective molecular-sieving gas separation membranes enabled by multi-covalent-crosslinking of microporous polymer blends. Nat Commun 12,6140 https://doi.org/10.1038/s41467-021-26379-5).
8. Baker, R. W.; Lokhandwala, K. (2008) Natural gas processing with membranes (2008) An overview. Ind. Eng. Chem. Res. 47(7) pp2109–2121
9. Lin, H.; White, L. S.; Lokhandwala, K. A.; Baker, R. W. (2013) Natural gas purification. In Encyclopedia of Membrane Science and Technology; Hoek, E. M. V., Tarabara, V. V., Eds. Wiley: Hoboken, NJ, p1644.
10. Baker, R. W (2014) Low, B. Gas separation membrane materials: A perspective. Macromolecules 47, 6999. Macromolecules, 47, pp6999-7013, DOI:10.1021/MA501488S
11. Lin, H. Integrated membrane material and process development for gas separation. Curr. Opin. Chem. Eng. 2014, 4, 54.
12. Nuradeen Labaran Tanko (2018) The effect of porosity on tortuosity, International Journal of Scientific & Engineering Research, 9 (6) pp2163-2169.
13. Mr. Padeepz (2018) DARCY'S LAW – Coefficient of Permeability
14. Hurwitz MF (1989) Flows through porous tubes-the end cap problem. In: Proceedings from mathematical problems in industry workshop.
15. Sanaei P, Richardson GW, Witelski TP, Cummings LJ (2016) Flow and fouling in a pleated membrane filter. J Fluid Mech 795, pp36-59
16. Griffiths IM, Howell PD, Shipley RJ (2013) Control and optimization of solute transport in a thin, porous tube. Physics Fluids 25(3):033101 (1994-present).
17. Ash R, Barrer RM. Mechanisms of surface flow Surface Science. 8: 461-466):

18. Merkel T. C., Bondar V. I., Nagai K., Freeman B. D. and Pinnau I. (2000) Gas sorption, diffusion, and permeation in poly(dimethylsiloxane) Journal of Polymer Science, Part B: Polymer Physics 38(3) pp415-434.
19. Xu, J., Vaillant, R. & Attinger, D. (2010) Use of a porous membrane for gas bubble removal in microfluidic channels: physical mechanisms and design criteria. Microfluid Nanofluid 9, pp765–772, https://doi.org/10.1007/s10404-010-0592-5.